Pergamon

Journal of Structural Geology, Vol. 18, No. 5, pp. 643 to 655, 1996

0191-8141/96 $15.00+0.00

0191-8141(95)00123-9

Computer simulation of single-layer buckling*

Y. ZHANG, B. E. HOBBS, A. ORD and H. B. MÜHLHAUS

Australian Geodynamics Cooperative Research Center, CSIRO Division of Exploration and Mining, Private Bag, Wembley, WA 6014, Australia

(*Received* 24 *October* 1994; *accepted in revised form* 3 *October* 1995)

Abstract—This paper aims to clarify the influence that initial perturbations have in controlling the buckling process. The questions are: how is the Biot–Ramberg dominant wavelength modified by the presence of finite initial perturbations? How is the shape of the resultant folds influenced by the initial geometry? In answering these questions we also revisit many of the results already embedded in the literature for viscous materials but contrast the behaviour of these materials with those of strongly pressure-dependent elastic–plastic materials; this paper represents the first time that the buckling behaviour of such materials has been reported. For layers with a series of initial small perturbations, the current results confirm that fold wavelength and growth rate are controlled by competence contrast (R). Wavelength selection also occurs in a layer involving perfectly-sinusoidal small perturbations, resulting in a dominant wavelength different from the input one. For layers with an isolated initial perturbation, both R and initial perturbation geometries influence buckling. If the width of the initial perturbation is smaller than a critical width related to R, significant growth of the initial perturbation is possible. When the width of the initial perturbation is larger than the critical width, the simple growth of the perturbation is possible only for early stages. It then splits into two or more secondary perturbations according to R. These perturbations can all grow into finite folds in elastic–viscous models, but only some of them can do so in elastic–plastic models. Copyright © 1996 Elsevier Science Ltd

INTRODUCTION

Single-layer buckling has attracted the attention of theoreticians and experimentalists for nearly half a century. Its understanding is considered to be a key step to interpreting the complexity of natural folding and deformation.

The most influential outcome from a vast number of such studies is the dominant wavelength theory, first proposed by Biot (e.g. 1957, 1959, 1961) and Ramberg (e.g. 1959, 1960, 1961) for viscous materials, then modified by others (e.g. Chapple 1968, 1969, Sherwin & Chapple 1968, Hudleston 1973a,b, Fletcher 1974, 1977, Smith 1975, 1977); a similar wavelength equation was derived even earlier by several engineers for elastic materials (e.g. Goodier 1946, Bijlaard 1946). The theory predicts that a single layer with many random small perturbations embedded in a weaker matrix will develop into a regular fold train when subjected to layer parallel shortening. The dominant wavelength is determined by the competence contrast between the layer and the matrix, and by layer thickness. This theory is applicable only to early folding stages because infinitesimal deformation is assumed (see Biot 1965). However, Chapple (1968) suggested that the theory can be reasonably extrapolated to the finite folding stages where limb dip is below 15–20°. Treagus (1973, 1981) further showed that the theory is applicable to the situations where shortening is oblique to the layer, but the stress required increases with increasing the obliquity (also see Treagus 1988, Treagus & Sokoutis 1992). An interesting buckling feature has also been reported by Hudleston & Lan (1994) who showed that fold shapes (hinge sharpness and limb straightness) are relatively insensitive to competence contrast and the shape of initial perturbations but are affected by the stress exponent for power-law materials. Furthermore, for Newtonian, viscous materials, Dieterich (1969, 1970) and Dieterich & Carter (1969) analysed stress–strain distributions and cleavage development in folds using the finite element method, and showed that an initial perturbation with wavelength equal to the dominant wavelength is amplified into marked folds by layer parallel shortening.

In contrast to the theory above, the results from studying the development of a single, isolated, large-amplitude perturbation in a single layer (Cobbold 1975, 1977, Williams *et al.* 1978, Abbassi & Mancktelow 1990, 1992, Mancktelow & Abbassi 1992, Mühlhaus 1993), emphasize the importance of initial perturbations. Cobbold's paraffin wax experiments (Cobbold 1975) and finite element modelling (Cobbold 1977) show that buckling in such a system involves an amplification of the initial perturbation and progressive fold propagation sideways along the layer. This was verified by Mühlhaus' (1993) analytical results for an elastic layer in a viscous matrix. The domination of the gradual amplification of initial single perturbations was also demonstrated numerically by Williams *et al.* (1978) and experimentally by Abbassi & Mancktelow (1990, 1992); however, little or weak sideways fold propagation was reported. In

*Paper No. 27 of the AGCRC.

particular, Abbassi & Mancktelow (1990) show that the symmetry of the initial perturbation can even be inherited by the final folds. In summary, these studies suggest that when the amplitude of initial perturbations is large or finite (at least for the situation of a single perturbation), the geometry of the initial perturbation determines the final wavelength and fold shapes.

The geometrical nature of initial perturbations in a layer seems to be an important factor influencing fold evolution. For natural bedding and veins, irregular finite-amplitude perturbations could often exist before deformation. The buckling theory for single layers with isolated finite-amplitude perturbations, as developed by the authors above (Cobbold 1975, 1977, Williams *et al.* 1978, Abbassi & Mancktelow 1990, 1992, Mancktelow & Abbassi 1992, Mühlhaus 1993), may therefore be appropriate in explaining some natural folds. However, some important questions have not yet been fully considered, in particular: (1) what is the effect of competence contrast, combined with the influence of isolated initial large perturbations, in this situation; and (2) will an isolated finite-amplitude perturbation always simply amplify when the layer is compressed?

In this study, we focus on these questions using a numerical approach based on the computer code FLAC (Fast Lagrangian Analysis of Continua, Cundall & Board 1988). We start with the buckling of single layers with a series of periodic small perturbations, and then concentrate on the buckling of single layers with isolated single perturbations. Two different theoretical materials are considered in this model, namely elastic–viscous and elastic–plastic. This study is the first to simulate folding in a Mohr–Coulomb elastic–plastic material. Therefore, another interest of this study is to explore the difference in buckling between this material and viscous materials.

THEORETICAL BASIS

FLAC, the solid modelling code employed here is based on the finite difference method whereby the discretized equations are solved by a dynamic relaxation scheme (Cundall & Board 1988, Itasca Consulting Group, Inc. 1992). As for the accuracy of the approximation, there are no major differences between finite difference and finite element methods based on four-node quadrilateral meshes. However, FLAC incorporates a very efficient strategy for the handling of volumetric constraints. Also the relaxation technique is robust in connection with localization modelling. The code has been used for studies of graben faults (Cundall 1990), shear bands (Hobbs & Ord 1989, Hobbs *et al.* 1990, Ord 1990), fabric development in folds (Zhang *et al.* 1993), theoretical polycrystals (Zhang *et al.* 1994a,b) and ice (Wilson & Zhang 1994).

Elastic–viscous (Maxwell) and elastic–plastic (Mohr–Coulomb) material models have been adopted for the simulations presented here. The simplified constitutive equations for both models are described as follows.

Elastic–viscous (Maxwell) material

This material is equivalent to a combination of an elastic element and a Newtonian viscous element in series (see Jaeger & Cook 1979, p. 315, Ranalli 1987, p. 82, Turcotte & Schubert 1982, p. 337), in which the instantaneous elastic response and the viscous deformation are coupled; the total strain (ε_{ij}) is the sum of the elastic strain (ε^{e}_{ij}) and viscous strain (ε^{v}_{ij}). The elastic strain relates to stress (σ_{ij}) according to Hooke's law

$$\sigma_{ij} = 2G\varepsilon^{e}_{ij} + (K - \tfrac{2}{3}G)\,\delta_{ij}\varepsilon^{e}_{kk}, \tag{1}$$

where G, K and δ_{ij} are shear and bulk moduli and the Kronecker delta, respectively, and the viscous strain rate ($\dot{\varepsilon}^{v}_{ij}$) relates linearly to stress according to the Newtonian flow law

$$\sigma_{ij} = 2\eta\dot{\varepsilon}^{v}_{ij} - \tfrac{2}{3}\eta\,\delta_{ij}\dot{\varepsilon}^{v}_{kk}, \tag{2}$$

η being viscosity. This linear rheology describes the behaviour of materials which show instantaneous elasticity but flow viscously under small stresses and over a long period, and it can predict the irrecoverable deformation of rocks at high temperatures, slow strain rates and high confining pressures. Similar linear viscous constitutive relations have been extensively used in modelling of buckle folds (e.g. Biot 1959, Chapple 1968, Dieterich & Carter 1969, Treagus 1973, Williams *et al.* 1978). An important aspect of this constitutive behaviour is that the flow stress is only weakly pressure dependent through an activation volume term (see Nicolas & Poirier 1976).

Elastic–plastic material

Experimental studies of rock deformation show that under certain temperature, strain-rate and pressure conditions rocks can undergo large irrecoverable deformation without loss of continuity after a yield stress is reached (Griggs *et al.* 1960, Edmond & Paterson 1972, Jaeger & Cook 1979, p. 87, Ranalli 1987, p. 88). This deformation behaviour can be appropriately described by an elastic–plastic constitutive relation (Ord 1991, also see Vermeer & de Borst 1984, Jaeger & Cook 1979, p. 228, Turcotte & Schubert 1982, p. 294). The materials prescribed by this rheology behave initially elastically until the maximum shear stress reaches a critical value (yield stress), and then deform plastically to large strain; yielding follows the Mohr–Coulomb yield criterion so that the flow stresses are strongly pressure-dependent (Ord 1991). The total strain of the material is assumed to be composed of an elastic part and a plastic part. The elastic part is determined by Hooke's law (equation 1), while the plastic part is governed by a non-associated plastic flow law with constant or evolving cohesion (C), friction angle (ϕ) and dilation angle (ψ)

$$\dot{\varepsilon}^{p}_{ij} = \lambda\frac{\partial g}{\partial\sigma_{ij}}, \tag{3}$$

where $\dot{\varepsilon}^{p}_{ij}$ is the plastic strain rate tensor, g is the plastic potential function and λ is a non-negative scalar multi-

plier under yielding (λ can be calculated from the condition of yielding); see Vermeer & de Borst (1984) for a full description of the rheology.

There still exist uncertainties as to which mechanical flow law is appropriate for natural rock deformation. While power-law constitutive relations are more commonly considered appropriate for lower lithospheric levels (e.g. Kirby & Kronenberg 1987, Tsenn & Carter 1987), based on experimental data at relatively high temperatures and pressures, they do not describe the failure behaviour of rocks. A power-law fluid (also Newtonian and other linear viscous fluids) starts to flow at any stress: no critical stress is involved. Additional problems with the application of power-law creep theories include the wide range of experimentally-derived constant values and the extrapolation of data for experimental conditions and materials to natural rock deformation.

MODEL SPECIFICATION

The numerical assemblies used here are similar to those generally adopted in the single-layer buckling problem (e.g. Biot 1957, Ramberg 1961, Dieterich 1970), that is, a central competent layer embedded in a less competent matrix (Fig. 1a). The central layer, with a length/thickness ratio of 99:1 (198 × 2 m), is initially seeded with either a series of periodic small perturbations (Figs. 1a & b) or a single isolated perturbation with a larger amplitude (see Fig. 5). A numerical specimen is approximated by a finite difference mesh (Fig. 1c). The meshes adopted for our simulations have 198 × 50 finite difference elements (corresponding to a specimen size of 198 × 134 m).

To construct the model, the appropriate material properties must be assigned to the mesh. In addition to density, bulk and shear moduli, which are needed for all models, viscosity is also required for the elastic–viscous models, and cohesion, friction and dilation angles are required for the elastic–plastic models. For single-layer buckling, an important parameter is the *competence contrast* (R) between the central layer and the matrix, where *competence* may be described as a measure of material strength (for the definitions of *competence*, see Treagus 1988 and Treagus & Sokoutis 1992). This parameter is defined as the Young's modulus ratio (E_1/E_2) for elastic folds (e.g. Goodier 1946) and the viscosity ratio for viscous folds (e.g. Sherwin & Chapple 1968, Dieterich & Carter 1969, Hudleston 1973a, Treagus 1973, Smith 1979). However, Treagus & Sokoutis (1992) and Treagus (1993) show that viscosity varies in time and space for power-law viscous materials, and therefore the use of a constant viscosity ratio as competence contrast is only valid for linear viscous materials. For the elastic–viscous and elastic–plastic materials simulated here, viscosity ratio and cohesion ratio must be considered respectively in defining the competence contrast because they control the viscous part and the plastic part of bulk deformation. Since both materials incorporate elastic behaviour, bulk and shear moduli should also be considered. For a constant Poisson's ratio, the following relationship exists

$$\frac{E_1}{E_2} = \frac{K_1}{K_2} = \frac{G_1}{G_2}. \tag{4}$$

In this study, therefore, for simplicity, competence contrast is assumed constant throughout buckling, and is defined as

$$R = \frac{\eta_1}{\eta_2} = \frac{K_1}{K_2} = \frac{G_1}{G_2} \tag{5}$$

for the elastic–viscous models and

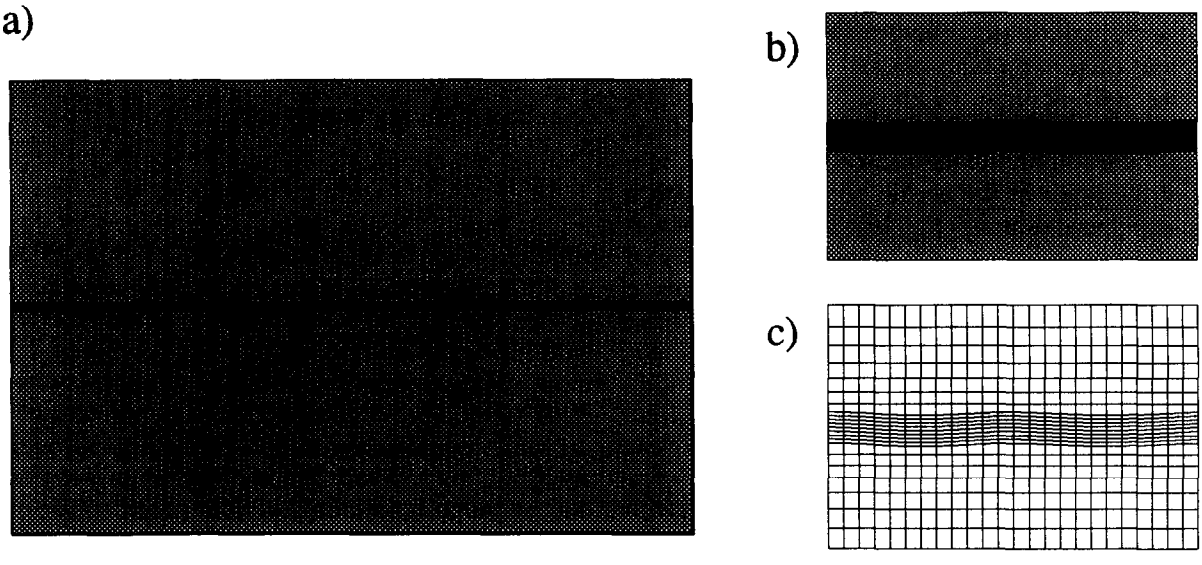

Fig. 1. (a) Geometry of a numerical model consisting of a central competent layer with a series of periodic small perturbations embedded in a less competent matrix. The model is actually plotted from a finite difference mesh formed of 198 × 50 elements. The small rectangle inside the specimen defines the area amplified in (b) and (c). (b) Amplified image of the defined small area in the model. (c) Part of the finite difference mesh, which constitutes the defined small area in the model.

$$R = \frac{C_1}{C_2} = \frac{K_1}{K_2} = \frac{G_1}{G_2} \tag{6}$$

for the elastic–plastic models, where subscripts 1 and 2 denote values for the layer and the matrix, respectively. The values R = 20, 50, 100 and 200 are adopted for the models presented in the following sections. To achieve these parameters, K_1, G_1, C_1 and η_1 are chosen as 2.3×10^{10}, 1.4×10^{10}, 2.0×10^9 Pa and 1.0×10^{20} Pa.s, respectively, and the properties for the matrix (η_2, K_2, G_2 and C_2) are then determined according to equations (4) and (5) for the adopted R values. A density of 2450 kg m^{-3} is used for both the layer and the matrix in all the simulations, and a friction angle of 30° and a dilation angle of 10° are incorporated in the elastic–plastic models (for the influence of ϕ and ψ on deformation, see Hobbs & Ord 1989, Ord 1990). The material properties for the central layer are close to those for sedimentary rocks (Clark 1966, Turcotte & Schubert 1982, p. 432). The current models assume a coherent, non-slip ('welded') contact between the layer and the matrix.

By use of velocity boundary conditions (VBC), all the numerical specimens are subjected to a pure shearing deformation with shortening parallel to the layer. The end deformation reached in the simulations ranges between 15 and 20% overall shortening; a simulation will stop if the deformation of any element in a mesh is so severe that the geometry of the element becomes numerically invalid. Adoption of stress boundary conditions could lead to results different to the VBC situation (Mühlhaus *et al.* 1994).

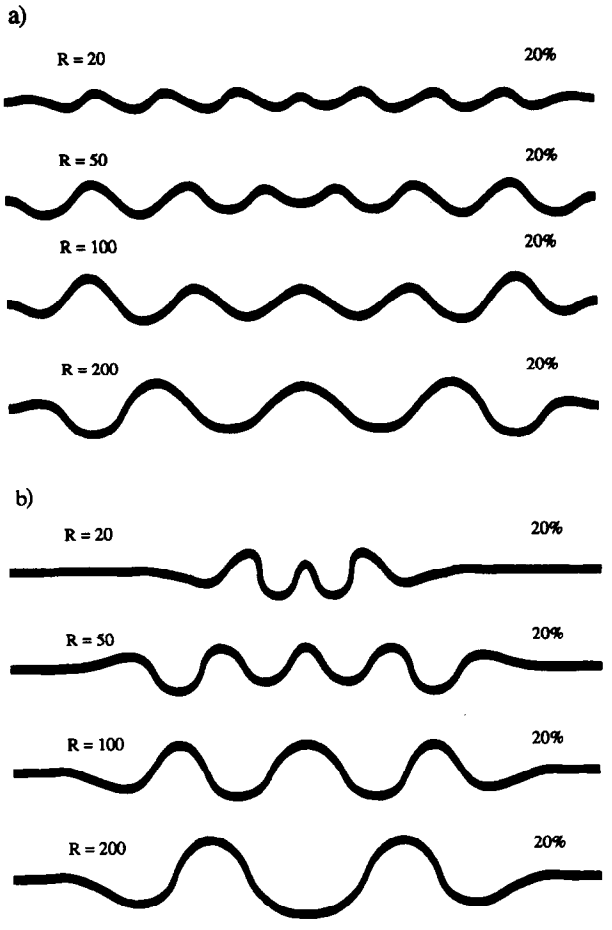

Fig. 2. Geometry of buckled single layers developed from the assembly with a central competent layer containing a series of periodic initial perturbations (see Fig. 1a). (a) Elastic–viscous material models. (b) Elastic–plastic material models. The R-values on the left side give competence contrast and the numbers on the right side show bulk shortening strains.

BUCKLING INVOLVING INITIAL PERIODIC SMALL PERTURBATIONS

In this group of simulations, a series of periodic small perturbations was introduced initially along the central layer (Fig. 1a), following the equation $y = 0.1 \sin(\pi x/6)$. These perturbations are equivalent to 16.5 full waveforms, and each has a limb dip of 1.9° (Fig. 1b), well below the limb-dip limit of about 5° for infinitesimal perturbations (Chapple 1968). The initial perturbations were introduced only in the central part (about one-third) of the layer in the elastic–plastic model with a small competence contrast (R = 20). This constraint was introduced to ensure that folds develop into the central part of the layer. Otherwise, the strain localization of the material causes the localized growth of folds in the regions near the ends of the layers, to which loading is applied.

Figure 2 shows the geometries of the buckled layers after 20% bulk shortening for eight models. A clear common feature for the elastic–viscous and elastic–plastic models is that the final wavelength increases with increasing competence contrast (also see Figs. 3a & d). The number of full waveforms (less than 7) for the final folds is much less than the number (16.5) for the initial perturbations. The fold amplitude (Figs. 2 and 3b & e) also increases with increasing competence contrast, similar to fold wavelength. These results are in line with the competency contrast–wavelength relationship predicted by the dominant-wavelength theory (e.g. Biot 1961, Ramberg 1961, Sherwin & Chapple 1968). The wavelengths achieved here are compared, in Table 1, with those calculated from the Biot–Ramberg equation (e.g. Biot 1961, equation 4.13)

$$L_d = 2\pi h \sqrt[3]{\frac{\eta_1}{6\eta_2}}, \tag{7}$$

where L_d is the dominant wavelength, h is the thickness of the competent layer, η_1 and η_2 are viscosity coefficients for the competent layer and the matrix, respectively. The maximum wavelengths of the elastic–viscous models, observed for an entire buckling history, are very close to the Biot–Ramberg dominant wavelengths for the same competence contrast, R; the final wavelengths are generally smaller than the maximum wavelengths due to bulk shortening and fold growth. The wavelengths of the elastic–plastic models also compare well with the Biot–Ramberg values for R = 20 and 50. For higher competence contrast (R = 100 and 200), however, the current wavelength values are clearly larger than the Biot–Ramberg values. This could reflect the

Table 1. Comparison between the wavelength achieved in this study and the dominant wavelength calculated from the Biot–Ramberg equation (e.g. Biot 1961, equation 4.13)

Competence contrast (R)	Biot–Ramberg dominant wavelength (m)	Wavelength of this study (m)			
		Elastic–viscous model		Elastic–plastic model	
		Maximum	Final	Maximum	Final
20	18.8	19.4	18.9	19.0	15.0
50	25.5	24.9	23.8	25.1	23.8
100	32.1	30.9	28.1	36.6	33.0
200	40.4	38.0	36.5	47.6	45.1

difference between the competence contrast defined for the elastic–plastic materials and that for the linear viscous materials.

The progressive development of fold wavelength and amplitude (Figs. 3a, b, d & e) shows that fold growth in both elastic–viscous and elastic–plastic materials is roughly exponential at first and then gradually slows down. Specifically, fold growth is very small in the early stages of deformation; wavelength and amplitude are stabilized at the values for the initial perturbations with small changes caused by layer-parallel shortening. However, after a certain amount of bulk shortening, 'explosive' fold growth which represents the onset of wavelength selection takes place. The sharp increases in wavelength and amplitude and therefore in fold growth rate occur within small strain increments. The timing of this 'explosive' growth relates to competence contrast (see Fig. 3). The larger the competence contrast, the smaller the bulk shortening at which the 'explosive' growth occurs. For example, the 'explosive' growth occurred after 14.6% overall shortening for the elastic–viscous model with $R = 20$, but it needed only 5.4% shortening for the model with $R = 200$. These results numerically confirm the 'explosive' manner of fold growth and its relevance to competence contrast as described by other authors (e.g. Biot 1961, Ramsay 1967, p. 378). Further development of folding after the 'explosive' stage is characterized by gradual slowing down. This growth feature is consistent with Mühlhaus *et al.*'s (1994) analytical results for the velocity boundary constraint. Mühlhaus *et al.* (1994) also show that, if stress boundary conditions are used, fold growth will be always exponential; this seems unlikely for natural folding.

There is a difference between the single layer buckling predicted here and that by the classic dominant-wavelength theory (e.g. Biot 1961). The geometry considered in the classic theory for wavelength selection is a layer with a series of small initial perturbations of various wavelengths, of which only those with the maximum growth rate are selected to grow. In contrast, the initial perturbations used here form a perfect sinusoid with a single wavelength of 12, much smaller than the Biot–Ramberg wavelengths (Table 1). According to the classic theory, these small perturbations would grow at the same rate since the rate is a function of the initial wavelength (also see Mancktelow & Abbassi 1992). Therefore, all the perturbations would grow into finite folds, and their wavelength would simply be the input wavelength, unrelated to the competency contrast; there would be no dominant wavelength. This is obviously not what occurred in the present models. The current results show that for such a starting geometry, a dominant wavelength still develops during the 'explosive' growth or wavelength selection stage. This dominant wavelength is different from the input one and is determined by the competency contrast. In early deformation stages, all the initial perturbations do grow at similar rates, each trying to achieve a dominant wavelength. However, this becomes impossible after a certain bulk shortening because the initial wavelength is too small to amplify in the layer according to the competency contrast. A selection process then occurs. This case may represent a special situation of dominant wavelength selection.

Another common feature of elastic–viscous and elastic–plastic buckling is that the variation of layer length (Figs. 3c & f) exhibits a two-stage pattern. The first is the layer-parallel shortening stage characterized by a gradual decrease in layer length; this stage has been widely described (e.g. Hudleston 1973a, Ramsay & Huber 1987, p. 392, Abbassi & Mancktelow 1992, Cruikshank & Johnson 1993). The second is the layer-parallel lengthening stage, in which the layer length increases. However, the lengthening in this stage is much smaller than the shortening in the earlier stage, and the layer lengths do not recover their original values by 20% bulk shortening. The change-over between the two stages roughly corresponds to the onset of the 'explosive' fold growth (Fig. 3). This indicates that the competence contrast determines the bulk shortening, at which the decrease in length switches to an increase. For the layer-matrix system with a small R-value, the layer-parallel shortening continues to a greater bulk shortening and reaches a greater value than the system with larger R-values.

The increase in layer length reported here is different from that observed in fold limbs during the late stages of folding as a result of flattening (e.g. Chapple 1968). A considerable part of the length increase takes place roughly along the whole layer while limb dip is still low. During the early shortening stages, strain is accommodated as an elastic component, and an elastic energy is accumulated accordingly. Once folding has initiated, release of the elastic energy becomes possible and the elastic strain component is recovered. This leads to some length increase relative to the shortened layer.

In spite of the essential similarity between the buck-

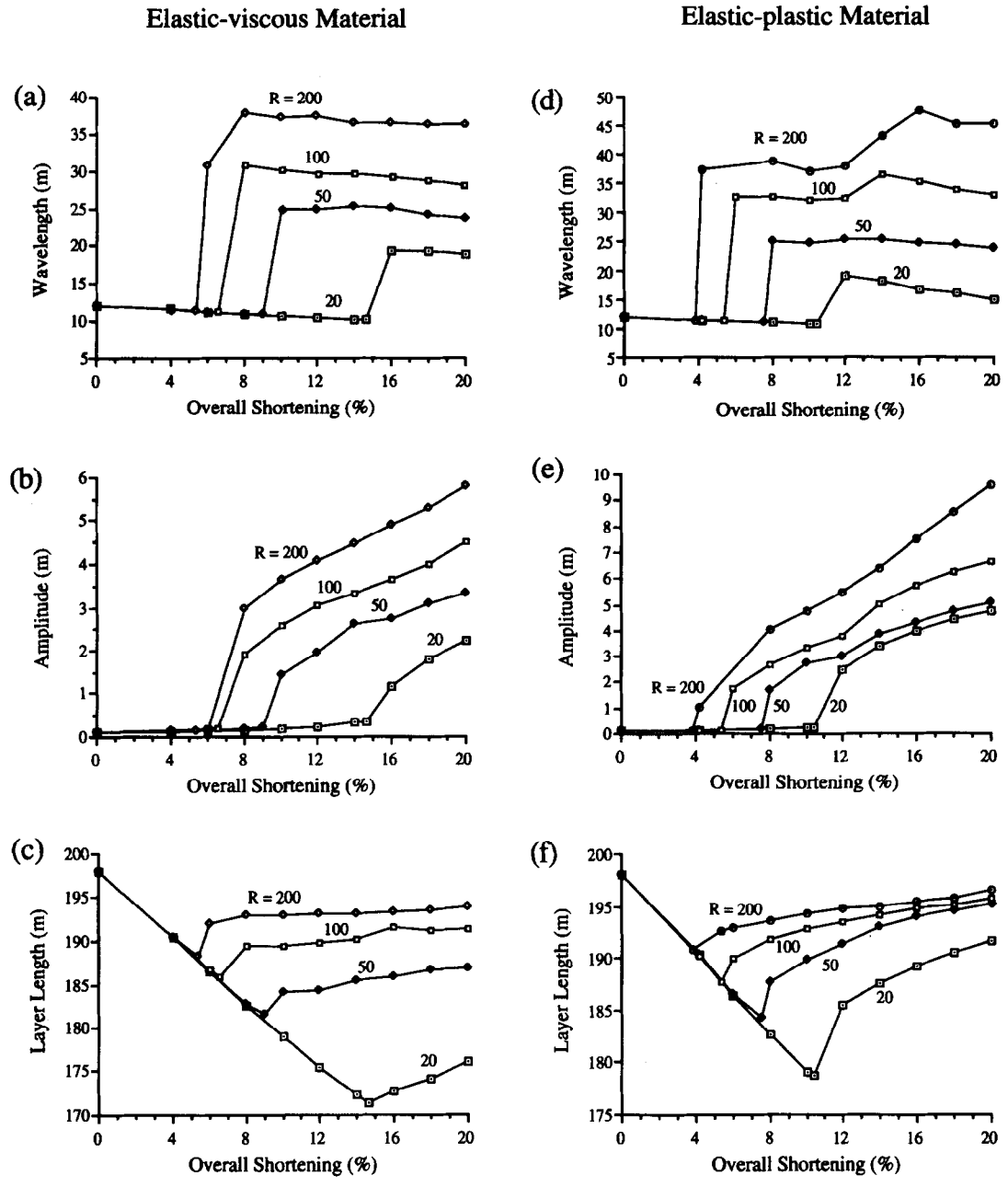

Fig. 3. Presentation of fold wavelength (a & d), amplitude (b & e) and layer length (c & f) vs bulk shortening strain for the buckled competent layers of elastic–viscous models (the left column) and elastic–plastic models (the right column). R is competence contrast. Starting geometry of the layers involves a series of periodic small perturbations.

ling results of the elastic–plastic and elastic–viscous models, some differences are also observed (Figs. 2 and 3). For a specific competence contrast, folds derived from the elastic–plastic models generally show larger amplitude, earlier occurrence of the 'explosive' growth and therefore smaller pre-buckling shortening than the corresponding elastic–viscous models. The wavelengths of the elastic–plastic models are also larger than the values of the elastic–viscous models for $R = 100$ and 200 (Table 1). But for $R = 20$ and 50, the wavelengths for the elastic–viscous and elastic–plastic models are rather close; the final wavelength of the elastic–plastic model with $R = 20$ is smaller due to the effect of localised buckling. Furthermore, the fold trains developed in the elastic–plastic models are less regular and have fewer buckles than in the elastic–viscous models. This difference is particularly evident in the models with $R = 20$. In this case, the buckling of the elastic–plastic layer is concentrated in the central part of the layer (Fig. 2b), and the resultant folds show a tighter or more angular geometry. This feature is related to the strain localization behaviour of the elastic–plastic material.

BUCKLING INVOLVING INITIAL SINGLE ISOLATED LARGER PERTURBATIONS

The following group of simulations was designed to investigate the amplification of single, isolated perturbations. The models are similar to that shown in Fig. 1(a), but the competent layer involves only a single, isolated, larger perturbation, rather than a series of

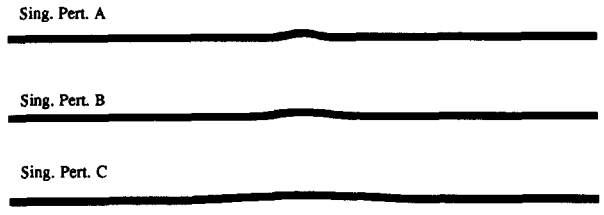

Fig. 4. Geometry of the central competent layers for three types of initial single isolated perturbations termed Sing. Pert. A, B and C, respectively. The numerical specimens are similar to that shown in Fig. 1(a) except for the change in the geometry of the central layer.

small perturbations. Three types of initial symmetric perturbations which bear some similarities to those used in Abbassi & Mancktelow's analogue experiments (1992) were considered here, termed perturbation A, B and C, respectively (Fig. 4). These three bell-shaped perturbations all have an initial amplitude of 1.4 m, but their widths are 14, 30 and 70 m, respectively; the limb dips are 10°, 5.3° and 2.5°, respectively. The simulations were performed for both the elastic–viscous and elastic–plastic materials, with $R = 20$ and 100. Another starting geometry, with an isolated asymmetric perturbation in the central layer (Fig. 7, the 0% stage), was also modelled, but only for the elastic–plastic material with $R = 100$. This asymmetric perturbation has an initial amplitude of 0.28 m and a width of 22 m; the limb dips are 1.1° and 2.2°.

Perturbations A and B

All the elastic–viscous and elastic–plastic models involving perturbations A and B (Fig. 4) demonstrate a consistent two-stage buckling feature (Figs. 5a–d and 6a–d) at 15–20% overall shortening. The early stage of folding is characterized by gradual amplification of the initial perturbations. During this stage the initial isolated perturbations grow into finite folds while the rest of the layer remains roughly flat. This kind of buckling geometry is quite similar to that shown by Williams *et al.* (1978) and Abbassi & Mancktelow (1990, 1992). However, this early stage does not persist beyond approximately 10% overall shortening for the models with $R = 20$, and 6% for the models with $R = 100$.

With further deformation, new perturbations formed in the rest of the layer away from the initial perturbation, through sideways propagation (e.g. see the 14% stage in Figs. 5a & c), while the central initial perturbation continued to grow; this is basically the result of the expansion of the flow field around the original perturbation along the layer. These new perturbations eventually grow into finite-amplitude folds that form fold trains together with the buckle grown from the initial perturbation. However, this fold propagation feature is not very clear for the elastic–plastic models with smaller R (e.g. 20) (Figs. 6a & c). The buckling development in this second stage correlates well with the progressive fold-propagation theory proposed by Cobbold (1975, 1977) and Mühlhaus (1993).

The factors controlling fold wavelength are different for the folds amplified from the initial isolated perturbations and for those developed through the process of sideways fold propagation. For the first category of folds, the width of the initial perturbations indeed influences the size of the final folds. The folds formed from the narrower initial perturbation A (see Figs. 5a & b and 6a & b) are also of shorter wavelength than the folds formed from the broader initial perturbation B (Figs. 5c & d and 6c & d). This can be more clearly illustrated by the values of final fold arc length (Table 2). That is, the folds grown from the perturbation B have larger arc length than those from the perturbation A. This feature is in good agreement with the results of previous studies (e.g. Cobbold 1975, Abbassi & Mancktelow 1990, 1992); Williams *et al.* (1978) also demonstrated that an initial single perturbation with a wavelength larger than the Biot wavelength leads to the formation of a fold broader than the Biot wavelength. However, the current results show that the competence contrast also influences the fold wavelength in this situation. For the same perturbation, a larger competence contrast results in a broader final fold with a larger final arc length (e.g. compare Figs. 5a & b and 6a & b; also see Table 2).

In contrast, the wavelength for the folds developed through sideways fold propagation is entirely determined by competence contrast, which is essentially the result of dominant wavelength selection. The simulations with $R = 100$ (Figs. 5b & d and 6b & d), as might be expected, consistently produced broader propagation folds than those formed in the models with $R = 20$ (Figs. 5a & c and 6a & c), irrespective of the width of the initial single perturbation. Taking the elastic–viscous models for example, in which fold propagation is particularly effective, the maximum wavelengths are 19.8 and 20.3 m for the models of $R = 20$ with perturbations A and B, respectively. These are clearly smaller than the values for the corresponding models with $R = 100$, 32.2 and 32.8 m, respectively. All these values are consistent with the Biot–Ramberg dominant wavelength for the same competence contrast, R (see Table 1).

Three major differences in the folding features are observed between the elastic–plastic and elastic–viscous models. First, the elastic–plastic models (Fig. 6) generally produce poorer fold-train geometries than the elastic–viscous models (Fig. 5). This is mainly due to strain localization associated with elastic–plastic materials. For such materials with a yield point, once deformation has localized in some areas and plastic yield has occurred, further deformation will preferentially continue in these areas. This behaviour significantly influences the folding process, so that the further buckling of the central layers is preferentially added to the growth of the pre-existing perturbations. Because of this fold localization, the formation of new perturbations along the layers and their growth are less prominent than in the elastic–viscous material. Secondly, the 'rate' of sideways fold propagation is different. For the elastic–plastic models, folds propagate 'slowly' over a large bulk shortening range, and therefore the process can be more clearly observed (e.g. Figs. 6b & d). In contrast, fold

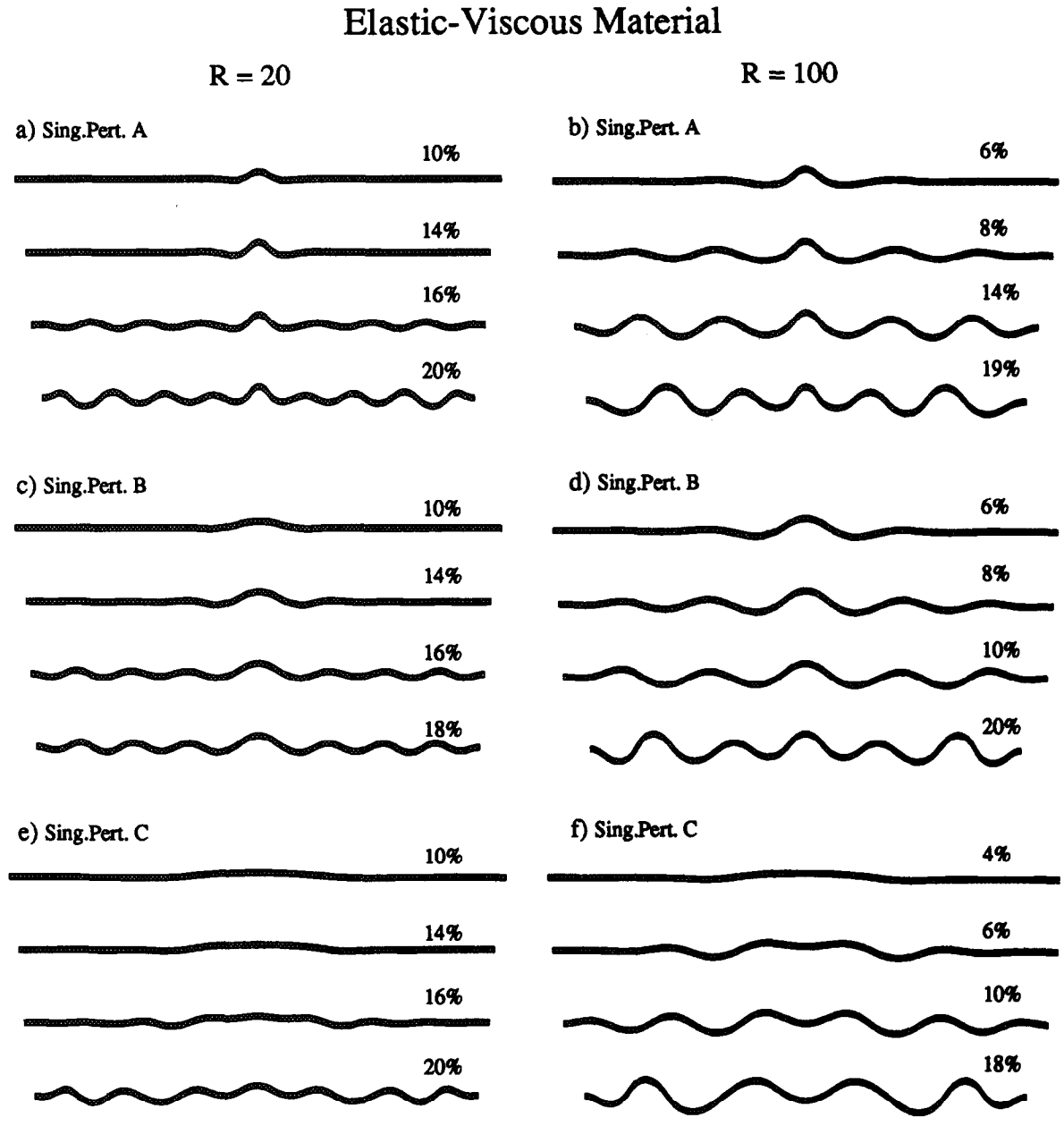

Fig. 5. Fold development in the central competent layers for elastic–viscous material models involving three types of initial single isolated perturbations (Sing. Pert. A, B and C). R is competence contrast.

propagation in the elastic–viscous models is much 'faster'. Fully-propagated folds are developed within a much smaller bulk shortening increment. Accordingly, the propagation is visible in only a certain deformation stage (e.g. the 14% stage in Fig. 5c). Finally, for the same initial perturbation and competence contrast, the fold wavelengths and arc lengths of the elastic–plastic models are larger than for the elastic–viscous model (see Figs. 5a–d and 6a–d and Table 2).

Perturbation C

As has been described above, perturbation C is an initial isolated perturbation much broader than perturbations A and B (see Fig. 4). Its width (70 m) is also significantly larger than the Biot–Ramberg wavelengths for $R = 20$ and 100 (see Table 1). The buckling development of the central layer for the models with perturbation C (Figs. 5e & f and 6e & f) is different from that for perturbations A and B.

All four simulations show that the simple amplification of the initial perturbation can be maintained only in the early buckling stages. The limb dips of the amplified perturbation at these stages have reached 8° (Fig. 5e, the 14% stage), 6° (Fig. 5f, the 4% stage), 5.6° (Fig. 6e, the 10% stage) and 7° (Fig. 6f, the 4% stage), respectively; these dips are all above the 5° limb dip limit for infinitesimal perturbations (Chapple 1968). However, with further deformation, the track of the perturbation development changes. The simple growth of the initial perturbation stops and new perturbations form within the original perturbation to accommodate additional layer-parallel shortening.

The further development of buckling is different for

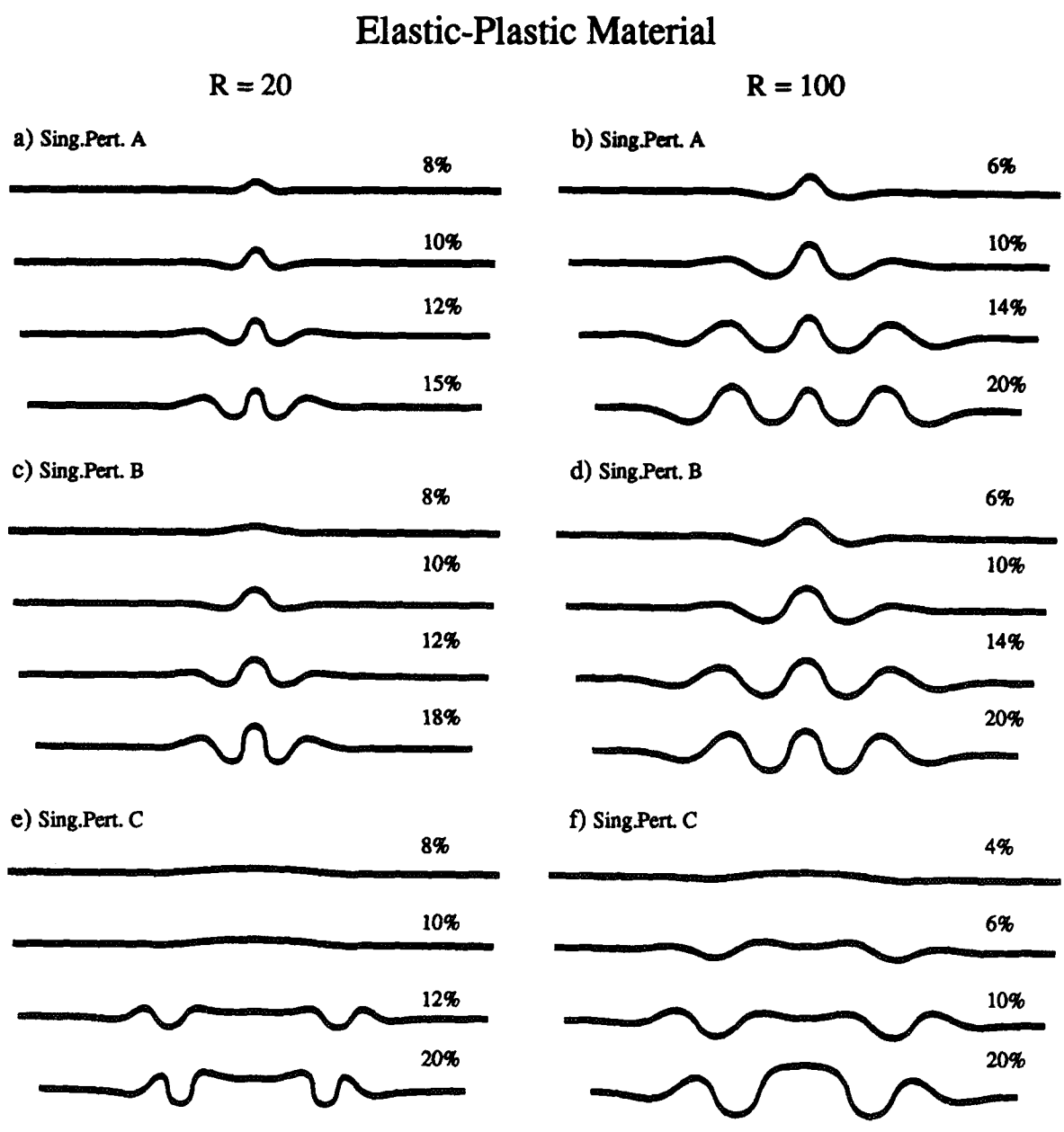

Fig. 6. Fold development in the central competent layers for elastic–plastic material models involving three types of initial single isolated perturbations (Sing. Pert. A, B and C). R is competence contrast.

Table 2. Final fold arc length for the folds amplified from the initial isolated single perturbations

Competence contrast (R)	Fold arc length (m)			
	Elastic–viscous model		Elastic–plastic model	
	Pert. A	Pert. B	Pert. A	Pert. B
20	23.9	35.1	30.4	36.7
100	31.0	38.9	40.1	44.0

the elastic–viscous and elastic–plastic models. In the elastic–viscous models, the original perturbation splits into three new perturbations in the run with $R = 20$ (Fig. 5e, the 16% stage) but into two new perturbations in the run with $R = 100$ (Fig. 5f, the 6% stage). The maximum wavelengths of these new perturbations are 18.7 and 29.4 m for $R = 20$ and 100, respectively, consistent with the Biot–Ramberg wavelengths (see Table 1) and also the wavelength results for the preceding elastic–viscous models. This would suggest that the wavelength of these secondary perturbations is totally controlled by the competence contrast, rather than by the size of the initial isolated perturbation C. As deformation continues, these secondary perturbations gradually amplify and eventually grow into finite folds. Simultaneously, new perturbations form and grow into finite folds in the

residual part of the layer outside the initial perturbation as a result of sideways fold propagation; this fold propagation is similar to perturbation A and B situations. The final result of the whole buckling process described above is a regular fold train (Figs. 5e & f). The trace of the initial perturbation C is barely distinguishable.

In the elastic–plastic models (Figs. 6e & f), the amplification development of the new secondary perturbations is different from that for the elastic–viscous models. As a result of strain localization, further buckling growth is concentrated on the two secondary perturbations generated near the two maximum dip points within the original perturbation, whereas there is little additional growth of folds in the middle part of the original perturbation. At the same time, the mechanism of sideways fold propagation creates two more perturbations, one to either side of the original perturbation, which are also able to grow. This kind of fold growth dominates the whole history and the final buckling product is an irregular fold train with a wide box fold in the central region (see Figs. 6e & f). Again, competence contrast significantly influences the wavelength of folds, which explains why the box fold formed passively in the model with $R = 20$ is wider than that in the model with $R = 100$; the central part of the layer displays a box-fold geometry as a result of secondary buckling at the limbs of the original perturbation.

The buckling behaviour of the layers with perturbation C are not in agreement with the general idea that initial perturbations will significantly grow if they have finite amplitudes (Williams *et al.* 1978, Abbassi & Mancktelow 1990, 1992, Mühlhaus 1993). We believe that the current result represents one of the important styles of growth of initial isolated perturbations. It seems that for a specific competence contrast there is a critical size limit for the isolated initial perturbations that can significantly amplify. If the width of an initial isolated perturbation is smaller than this limit (e.g. the perturbation A and B cases), their simple progressive growth, subject to the influence of competence contrast, should generally be possible. However, if the width of an initial isolated perturbation is too large (e.g. the perturbation C case), their simple growth is only possible in the early deformation stages. As deformation continues, the initiation and growth of new perturbations within the original perturbation occurs, with their geometry dependent on the competence contrast, as demonstrated by the current results. A quantitative determination of the relationship between this critical perturbation size limit and competency contrast requires the performance of a large number of numerical simulations, and will be the subject of follow-up work.

An asymmetric perturbation

This isolated asymmetric initial perturbation is barely distinguishable before deformation due to its small limb dips (Fig. 7). After 4% overall shortening, however, its asymmetric geometry becomes clearly visible. As the deformation continues, the asymmetric perturbation is gradually amplified into a high-amplitude asymmetric fold, manifested in its contrasting limb dips and thicknesses (see Fig. 7, the 18% stage). Fold propagation occurs along the layer outside the original perturbation, and the resulting folds also display an asymmetric geometry; note that the asymmetric fold grown from the initial perturbation is roughly symmetric to a propagated asymmetric fold on its right, and this could cause misreading of fold symmetry. These results are in good agreement with Abbassi & Mancktelow's experimental results (1990) and confirm that the symmetry of the initial perturbation does control the symmetry of the final folds.

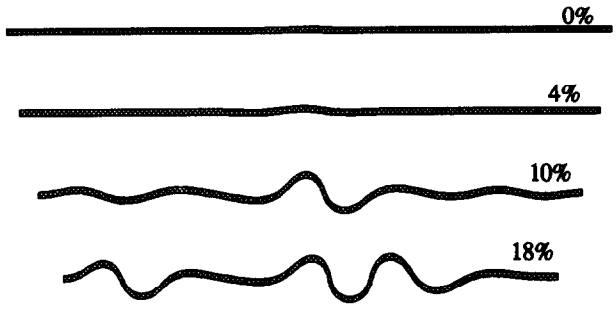

Fig. 7. Fold development of a central competent layer with an initial single asymmetric perturbation (elastic–plastic model and $R = 100$).

It should be noted that the initial isolated asymmetric perturbation of this model has initial limb dips of 1.1° and 2.2°, which falls into the range of the infinitesimal-amplitude perturbations (see Chapple 1968). This suggests that the symmetry of a single isolated perturbation can still control the symmetry of the final folds even though its amplitude is infinitesimal. Of course, the wavelength of the final folds should be mainly controlled by the competence contrast. We should mention that the fold asymmetry obtained here is weaker as compared to Abbassi & Mancktelow's (1990) experimental folds. This is probably because Abbassi & Mancktelow's initial asymmetric perturbations have a finite amplitude and therefore have stronger influence on the geometry of final folds.

DISCUSSION

Single layer buckling is essentially a process of the selection, amplification and propagation of initial perturbations, subject to the influence of competence contrast. In such a process, initial perturbations and competence contrast are two equally important factors. Their coexistence is the basic prerequisite for buckling. In fact, an indefinite number of possible combinations of both in natural situations is probably the main factor behind the complexity of natural folds.

Buckling following the dominant wavelength selection mechanism (e.g. Biot 1959, Ramberg 1961, Chapple 1968, Sherwin & Chapple 1968) represents only one standard situation where an infinite number of infinitesimal random perturbations is initially present in the layer. In this situation, all the initial perturbations are

subjected to a selection process and only some of them, namely those with maximum growth rate, can grow into finite folds; the wavelength is controlled by the competence contrast and layer thickness. Even if the initial infinitesimal perturbations are perfectly sinusoidal, additional harmonics could become activated as bulk shortening continues, due to the non-linear character of the constitutive relations (e.g. in connection with plastic yielding). Among these activated harmonics, a wavelength selection process takes place, leading to a single dominant wavelength and ultimately determining the appearance of the folds.

The dominant wavelength selection breaks down before the dip of limbs reaches 10–15° (Chapple 1968). This is basically because the dominant wavelength equation (see Biot 1959, Ramberg 1961), owing to its infinitesimal strain assumption, is not suitable for prediction of the wavelength change for further deformation. However, the selection process is effectively already completed and the framework of folds is thus defined by this stage. The later variation of wavelength reflects only the effect of kinematic shortening (see Figs. 3a & d). The dominant wavelength buckling theory is important because it reveals the mechanism of wavelength selection and the relationship between wavelength and competence contrast. This relationship could be used to estimate rheologic parameters for naturally folded rocks (Fletcher 1974, Hudleston & Lan 1994).

The buckling of single layers with a single isolated perturbation represents a different situation, which may also be well approximated by layers with a limited number of well-separated perturbations. Here the geometry of the initial perturbation comes to play a more important role in the process of buckling, particularly when the amplitude of the perturbation is finite (e.g. Cobbold 1975, Williams *et al.* 1978, Abbassi & Mancktelow 1990, 1992). The geometry (e.g. symmetry) of the initial perturbation can significantly influence the geometry of the final fold that grows from the initial perturbation. This conclusion seems to hold true even when the initial isolated perturbation is infinitesimal (see Fig. 7). This is understandable since the simple amplification of the perturbation is the easiest way to start buckling.

Nevertheless, competence contrast still influences the buckling in this situation. The significant growth of the initial isolated perturbation (e.g. Abbassi & Mancktelow 1990, 1992, Mühlhaus 1993) is generally possible if the width of the initial perturbation is equal to or smaller than a critical width for the involved competence contrast (the perturbation A and B cases). This is probably because the buckling growth of an initial perturbation of this size is sustainable for this competence contrast. The final fold wavelength in this case is also influenced by the competence contrast; the competency contrast influences the growth rate of the initial isolated perturbation (Abbassi & Mancktelow 1992, Mancktelow & Abbassi 1992). In particular, the sideways propagation of folds in the rest of the layer outside the initial perturbation, and their wavelength, are chiefly determined by the competence contrast (see Figs. 5a–d and 6a–d). The simple growth of the initial perturbation is unlikely when the width of the initial perturbation in the layer exceeds the critical width for the corresponding competence contrast (the perturbation C case). Growth on the scale of such an initial perturbation is simply not allowed by the buckling ability of the layer, which is determined by the competence contrast. The buckling should then follow the development of the C type perturbation (see Figs. 5e & f and 6e & f). That is, the perturbation shows some growth at early stages and then splits into separate, smaller perturbations that can further develop into folds. A precise specification of the relationship between competence contrast and the critical perturbation width discussed above is not possible at this stage, owing to the limited number of simulations performed. However, a full definition of this relationship is possible through continued work in this direction.

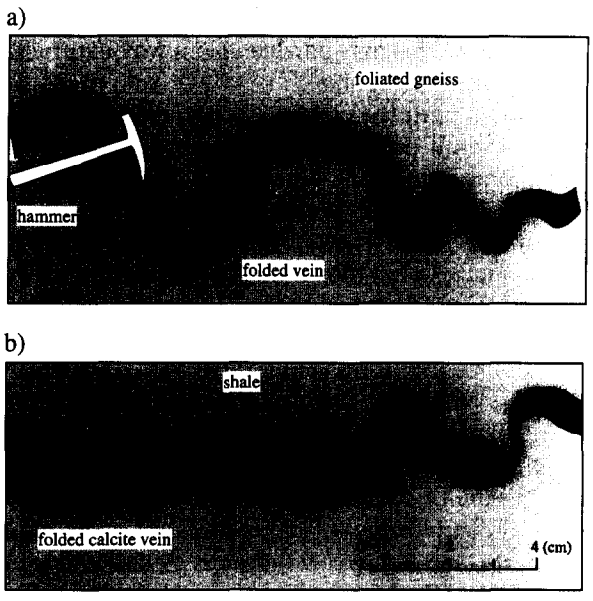

Fig. 8. Examples of natural folds. (a) A folded vein in foliated gneiss, Lower Paleozoic, near Korgen, Nordland, Norway (after Weiss 1972, plate 171). (b) A folded calcite vein in shale, Cinque Terra, Italy (after Abbassi & Mancktelow 1990, fig. 3).

Features of the models with perturbation C may be important to understanding some natural folds. Figure 8 gives two examples of natural folds (see Weiss 1972, plate 171, Abbassi & Mancktelow 1990, fig. 3). The box-like geometries of these natural folds in veins compare well with those developed in the current elastic–plastic models involving the C-type perturbation (Figs. 6e & f). The development of these natural folds may be similar to that responsible for fold development in the models; the widths of the possible initial perturbations may have exceeded the critical values allowed by the buckling ability of the veins. In a more general sense, natural bedding or a vein could often have a number of finite-amplitude initial perturbations of various widths, as caused by a particular sedimentary environment or irregular spacing of tensile fractures. Buckling of such a system should produce an irregular fold train if the geometry of the initial perturbation and competence

contrast both influence the process in the way predicted by this study. This may partly explain why natural folds are mostly very irregular.

Although both the elastic–viscous and elastic–plastic models overall predict a consistent buckling development, some important differences do exist, as noted above. For the elastic–viscous materials, it seems that a roughly regular fold train can always be developed in the end, no matter what the initial geometries are involved. In contrast, the buckling of the elastic–plastic materials is more influenced by the initial geometries and produces poorer fold-train geometries.

It is not yet clear which rheological model (elastic–plastic, elastic–viscous, Newtonian viscous and power-law viscous) best suits natural folds. This is mainly due to the uncertainty about the mechanical flow laws appropriate to complex geological conditions, as mentioned above (also see Treagus & Sokoutis 1992, Hudleston & Lan 1994). However, we suggest that the buckling results of the elastic–plastic models are applicable to folding of rocks in the upper crust (see Ord 1991), based on the following considerations. (1) The poorer fold trains predicted by the elastic–plastic models compare better with fold irregularity often observed in the upper crust. (2) The fold geometries achieved in the elastic–plastic models with isolated initial perturbations agree better with some natural folds (Weiss 1972) and experimental folds (Abbassi & Mancktelow 1990, 1992). (3) The yielding behaviour incorporated in the models simulates well the failure behaviour of rocks (Griggs *et al.* 1960, Edmond & Paterson 1972, Jaeger & Cook 1979). (4) The elastic–plastic rheology is suggested as being appropriate to model the ductile behaviour of rocks at low temperatures (Jaeger & Cook 1979, p. 228, Vermeer & de Borst 1984, Ord 1991).

The elastic–viscous and other (non-linear) viscous rheologies may be more appropriate to model rock behaviour at high temperatures (a significant fraction of the melt temperature; e.g. Turcotte & Schubert 1982, p. 296) or deeper lithospheric levels (Ord 1991). These conditions may be less common in the shallow crust.

CONCLUSIONS

For the buckling of single layers with a series of initial periodic small perturbations, the current numerical results agree well with the dominant wavelength selection theory. Fold wavelength is controlled by competency contrast when layer thickness is fixed. Fold growth is exponential at first and then gradually slows down. The variation of layer length exhibits a two-stage pattern, that is, layer-parallel shortening followed by certain layer-parallel lengthening. The degree of bulk shortening for the change-over between both is dependent on competence contrast. It is also shown that wavelength selection occurs in a layer with a series of perfectly-sinusoidal small perturbations. This process leads to a dominant wavelength after a certain bulk shortening.

For layers containing single isolated initial perturbations, competence contrast and initial perturbation geometry both influence buckling. When the width of the initial perturbations is smaller than a critical width for a particular competence contrast, the initial perturbation can grow significantly, subject to a certain influence of the competence contrast. The geometry (e.g. symmetry) of the initial perturbation controls the geometry of the final fold. However, if the width of the isolated initial perturbation exceeds the critical value allowed by the buckling capacity of the layer, which is determined by the competence contrast, then simple growth of the initial perturbation is possible only for early deformation stages. The perturbation then splits into two or more secondary perturbations according to the competence contrast. These secondary perturbations can all grow into finite folds in the elastic–viscous models, but only some of them can do so in the elastic–plastic models which display strain localisation. Fold propagation sideways along the layer outside the initial perturbation is so well developed in the elastic–viscous models that a regular fold train can always form in the end. In contrast, the elastic–plastic materials show poorer propagation and therefore develop poorer fold-train geometries. The wavelength of propagation-formed folds is controlled entirely by competence contrast.

Acknowledgements—N. S. Mancktelow, P. J. Hudleston, S. H. Treagus and M. Craig are thanked for their thorough reviews, and critical and constructive comments, from which this paper has greatly benefited. We acknowledge ITASCA for use of the code FLAC. This paper is published with the permission of the Director of AGCRC.

REFERENCES

Abbassi, M. R. & Mancktelow, N. S. 1990. The effect of initial perturbation shape and symmetry on fold development. *J. Struct. Geol.* **12**, 273–282.

Abbassi, M. R. & Mancktelow, N. S. 1992. Single layer buckle folding in non-linear materials—I. Experimental study of fold development from an isolated initial perturbation. *J. Struct. Geol.* **14**, 85–104.

Bijlaard, P. P. 1946. On the elastic stability of thin plates supported by a continuous medium. *Proc. K. Ned. Akad. Wet.* **49**, 1189–1199.

Biot, M. A. 1957. Folding instability of a layered viscoelastic medium under compression. *Proc. R. Soc. Lond.* **A242**, 444–454.

Biot, M. A. 1959. On the instability of folding deformation of a layered viscoelastic medium in compression. *J. appl. Mech.* **26**, 393–400.

Biot, M. A. 1961. Theory of folding of stratified viscoelastic media and its implications in tectonics and orogenesis. *Bull. geol. Soc. Am.* **72**, 1595–1620.

Biot, M. A. 1965. *Mechanics of Incremental Deformations*. John Wiley & Sons, New York.

Chapple, W. M. 1968. A mathematic theory of finite-amplitude rock-folding. *Bull. geol. Soc. Am.* **79**, 47–68.

Chapple, W. M. 1969. Fold shape and rheology: the folding of an isolated viscous-plastic layer. *Tectonophysics* **7**, 97–116.

Clark, S. P., Jr. (editor) 1966. *Handbook of Physical Constants. Mem. geol. Soc. Am.* **97**.

Cobbold, P. R. 1975. Fold propagation in single embedded layers. *Tectonophysics* **27**, 333–351.

Cobbold, P. R. 1977. A finite-element analysis of fold propagation—a problematic application. *Tectonophysics* **38**, 339–353.

Cruikshank, K. M. & Johnson, A. M. 1993. High-amplitude folding of linear-viscous multilayers. *J. Struct. Geol.* **15**, 79–94.

Cundall, P. A. 1990. Numerical modelling of jointed and faulted rock. In: *Proceedings of Int. Conf. on Mechanics of Jointed and Faulted Rock*, 11–18.

Cundall, P. A. & Board, M. 1988. A microcomputer program for

modelling large-strain plasticity problem. In: *Numerical Methods in Geomechanics* (edited by Swobada, C.). *Proc. 6th Int. Conf. on Numerical Methods in Geomechanics*. Balkema, Rotterdam, 2101–2108.

Dieterich, J. H. 1969. Origin of cleavage in folded rocks. *Am. J. Sci.* **267**, 155–165.

Dieterich, J. H. 1970. Computer experiments on mechanics of finite amplitude folds. *Can. J. Earth Sci.* **7**, 467–475.

Dieterich, J. H. & Carter, N. L. 1969. Stress-history of folding. *Am. J. Sci.* **267**, 129–154.

Edmond, J. M. & Paterson, M. S. 1972. Volume changes during the deformation of rocks at high pressures. *Int. J. Rock Mech. & Min. Sci.* **9**, 161–182.

Fletcher, R. C. 1974. Wavelength selection in the folding of a single layer with power-law rheology. *Am. J. Sci.* **274**, 1029–1043.

Fletcher, R. C. 1977. Folding of a single viscous layer: exact infinitesimal amplitude solution. *Tectonophysics* **39**, 593–606.

Goodier, J. N. 1946. Cylindrical buckling of sandwich plates. *J. appl. Mech., Trans. ASME* **68**, 253–260.

Griggs, D. T., Turner, F. J. & Heard, H. C. 1960. Deformation of rocks at 500° and 800°C. In: *Rock Deformation. Mem. geol. Soc. Am.* **79**, 39–104.

Hobbs, B. E. & Ord, A. 1989. Numerical simulation of shear band formation in a frictional-dilational material. *Ingenieur-Archiv* **59**, 209–220.

Hobbs, B. E., Mühlhaus, H.-B., & Ord, A. 1990. Instability, softening and localisation of deformation. In: *Deformation Mechanisms, Rheology and Tectonics* (edited by Knipe, R. J. & Rutter, E. H.). *Spec. Publs. geol. Soc. Lond.* **54**, 143–165.

Hudleston, P. J. 1973a. An analysis of "single-layer" folds developed experimentally in viscous media. *Tectonophysics* **16**, 189–214.

Hudleston, P. J. 1973b. Fold morphology and some geometrical implications of theories of fold development. *Tectonophysics* **16**, 1–46.

Hudleston, P. J. & Lan, L. 1993. Information from fold shapes. *J. Struct. Geol.* **15**, 253–264.

Hudleston, P. J. & Lan, L. 1994. Rheological controls on the shapes of single-layer folds. *J. Struct. Geol.* **16**, 1007–1021.

Itasca Consulting Group, Inc. 1992. *FLAC: Fast Lagrangian Analysis of Continua, User Manual, Version* 3.2. Itasca Consulting Group, Inc., Minneapolis.

Jaeger, J. C. & Cook, N. G. W. 1979. *Fundamentals of Rock Mechanics*. Chapman and Hall, London.

Kirby, S. H. & Kronenberg, A. K. 1987. Rheology of the lithosphere: selected topics. *Rev. Geophys.* **25**, 1219–1244.

Mancktelow, N. S. & Abbassi, M. R. 1992. Single layer buckle folding in non-linear materials—II. Comparison between theory and experiment. *J. Struct. Geol.* **14**, 105–120.

Mühlhaus, H. B. 1993. Evolution of elastic folds in plane strain. In: *Modern Approaches to Plasticity* (edited by Kolymbas, D.). Elsevier, Amsterdam, 737–765.

Mühlhaus, H. B., Hobbs, B. E. & Ord, A. 1994. The role of axial constraints on the evolution of folds in single layers. In: *Computer Methods in Geomechanics* (edited by Siriwardane, H. J. & Zaman, M. M.). Balkema, Rotterdam, 223–231.

Ord, A. 1990. Mechanical controls on dilatant shear zones. In: *Deformation Mechanisms, Rheology and Tectonics* (edited by Knipe, R. J. & Rutter, E. H.). *Spec. Publs geol. Soc. Lond.* **54**, 183–192.

Ord, A. 1991. Deformation of rock: A pressure-sensitive, dilatant material. In: *Localization of Deformation in Rocks and Metals* (edited by Ord, A., Hobbs, B. E. & Mühlhaus, H.-B.). *Pure & Appl. Geophys.* **137**, 337–366.

Nicolas, A. & Poirier, J. P. 1976. *Crystalline Plasticity and Solid State Flow in Metamorphic Rocks*. Wiley, New York.

Ramberg, H. 1959. Evolution of ptygmatic folding. *Norsk geol. Tidsskr.* **39**, 99–151.

Ramberg, H. 1960. Relationship between length of arc and thickness of ptygmatically folded veins. *Am. J. Sci.* **258**, 36–46.

Ramberg, H. 1961. Contact strain and folding instability of a multilayered body under compression. *Geol. Rdsch.* **51**, 405–439.

Ramsay, J. G. 1967. *Folding and Fracturing of Rocks*. McGraw-Hill, New York.

Ramsay, J. G. & Huber, M. I. 1987. *The Techniques of Modern Structural Geology, Volume* 2: *Folds and Fractures*. Academic Press, London.

Ranalli, G. 1987. *Rheology of the Earth*. Allen & Unwin, London.

Sherwin, J. A. & Chapple, W. M. 1968. Wavelengths of single layer folds: a comparison between theory and observation. *Am. J. Sci.* **266**, 167–179.

Smith, R. B. 1975. Unified theory of the onset of folding, boudinage and mullion structure. *Bull. geol. Soc. Am.* **86**, 1601–1609.

Smith, R. B. 1977. Formation of folds, boudinage and mullions in non-Newtonian materials. *Bull. geol. Soc. Am.* **88**, 312–320.

Smith, R. B. 1979. The folding of a strongly non-Newtonian layer. *Am. J. Sci.* **279**, 272–287.

Treagus, S. H. 1973. Buckling stability of a viscous single-layer system oblique to the principal compression. *Tectonophysics* **19**, 271–289.

Treagus, S. H. 1981. A theory of stress and strain variations in viscous layers, and its geological implications. *Tectonophysics* **72**, 75–103.

Treagus, S. H. 1988. Strain refraction in layered system. *J. Struct. Geol.* **10**, 517–527.

Treagus, S. H. 1993. Flow variation in power-law multilayers: implication for competence contrasts in rocks. *J. Struct. Geol.* **15**, 423–434.

Treagus, S. H. & Sokoutis, D. 1992. Laboratory modelling of strain variation across rheological boundaries. *J. Struct. Geol.* **14**, 405–424.

Tsenn, M. C. & Carter, N. L. 1987. Upper limits of power law creep of rocks. *Tectonophysics* **136**, 1–26.

Turcotte, D. L. & Schubert, G. 1982. *Geodynamics: Applications of Continuum Physics to Geological Problems*. Wiley, New York.

Vermeer, P. A. & de Borst, R. 1984. Non-associated plasticity for soils, concrete and rock. *Heron* **29**, 1–64.

Weiss, L. E. 1972. *The Minor Structures of Deformed Rocks*. Springer, Berlin.

Williams, J. R., Lewis, R. W. & Zienkiewicz, O. C. 1978. A finite-element analysis of the role of initial perturbations in the folding of a single viscous layer. *Tectonophysics* **45**, 187–200.

Wilson, C. J. L. & Zhang, Y. 1994. Comparison between experiment and computer modelling of plane strain simple shear ice deformation. *J. Glaciol.* **40**, 46–55.

Zhang, Y., Hobbs, B. E. & Jessell, M. W. 1993. Crystallographic preferred orientation development in a buckled single layer: a computer simulation. *J. Struct. Geol.* **15**, 265–276.

Zhang, Y., Hobbs, B. E. & Jessell, M. W. 1994a. The effect of grain boundary sliding on fabric development in polycrystalline aggregates. *J. Struct. Geol.* **16**, 1315–1325.

Zhang, Y., Hobbs, B., E. & Ord, A. 1994b. A numerical simulation of fabric development in polycrystalline aggregates with one slip system. *J. Struct. Geol.* **16**, 1297–1313.